Research Article

Explicit incompressible SPH algorithm for modelling channel and lid-driven flows

Morteza Bayareh[1] · Amireh Nourbakhsh[2] · Fardin Rouzbahani[2] · Vahid Jouzaei[2]

Abstract
In this paper, explicit incompressible Smoothed Particle Hydrodynamics (ISPH) algorithm is used to simulate two-dimensional channel flow, channel flow in the presence of a square solid object and lid-driven square cavity flow for both Newtonian and non-Newtonian fluids. It is demonstrated that 2640 particles are sufficient to predict the behavior of channel flow. As the power low index decreases, more iteration is needed to reach steady state conditions. The results reveal that only 1600 particles are required for reasonable prediction of lid-driven square cavity flow at Re = 100 and 400 and 6400 particles is required to predict it at Re = 1000. It is also concluded that the ISPH method has a high ability to predict the behavior of non-Newtonian power law fluids.

Keywords Smoothed particle hydrodynamics (SPH) method · Incompressible SPH · Three-phase algorithm · Channel flow · Lid-driven cavity flow

List of symbols

D	Deformation tensor
g	Acceleration due to gravity (m/s^2)
h	Smoothing length (m)
H	Channel width (m)
L	Channel length (m)
L_0	Initial particle distance (m)
m	Mass (kg)
n	Power law index
P	Pressure (Pa)
r_{ij}	Distance between the particles i and j (m)
Re	Reynolds number
t	Time (s)
u	Velocity vector (m/s)
V	Volume of particle (m^3)
W_n	Kernel function
x, y	Coordinates (m)

Greek symbols

ρ	Density (kg/m^3)
μ	Viscosity (Ns/m^2)
μ_{eff}	Effective viscosity (Ns/m^2)
τ	Shear stress (Pa)

1 Introduction

Smoothed Particle Hydrodynamics (SPH) method is the oldest meshless Lagrangian method developed in 1977 by Lucy [1] and Gingold and Monaghan [2] to solve numerical problems of gas dynamics. In the SPH method, the governing equations are discretized by interpolating the flow properties in spatially distributed particles (pseudo-particles) that are irregularly dispersed in the flow field without the need for mesh generation. The SPH method is a Lagrangian method in which the fluid is dispersed into many particles that move with the flow velocity. As a meshless Lagrangian method, SPH has several advantages over the other methods. Since the particles carry their own properties, the fluid flow is easily represented by the motion of these particles. This is exhibited in the simulation of a two-phase flow by assigning each particle to its

✉ Amireh Nourbakhsh, nourbakhsh@basu.ac.ir | [1]Department of Mechanical Engineering, Shahrekord University, Shahrekord, Iran. [2]Department of Mechanical Engineering, Bu-Ali Sina University, Hamedan, Iran.

SN Applied Sciences (2019) 1:1040 | https://doi.org/10.1007/s42452-019-1072-5

Received: 9 July 2019 / Accepted: 9 August 2019 / Published online: 16 August 2019

own phase. In this method, various fluid properties such as density, velocity and pressure are known. The value of a dependent variable is also calculated by accumulating a series of adjacent particles. Differential equations are converted to integral equations using an interpolation function. Instead of physical quantities, spatial derivatives act on an interpolation function that is an analytic and derivative function [3].

SPH is a suitable approach for modeling the flows with a complex free surface. Due to the Lagrangian nature of this method, the advection terms that cause the numerical diffusion errors do not appear in the equations. The main challenge of weak compressible SPH (WCSPH) methods is the production of pressure oscillations in the computational flow field.

In the past two decades, many attempts have been made to simulate different problems using the SPH method: compressible, incompressible, and free-surface flows [4], viscid flows [5] and low-Reynolds-number flows [6]. Monaghan [4] for the first time applied the SPH method to simulate an incompressible free-surface fluid flow. Monaghan [7] proposed a hypothetical pressure to produce a relatively small repellent force for numerical resolution stability. Monaghan [8] also presented a turbulence version of the SPH method for simulating compressible flows with variable particle separation in time and place. Liu et al. [9] examined wave propagation on a coastal structure using SPH method. Ellero et al. [10] introduced another model for incompressible flows. In this model, a constant volume of fluid particles is obtained by establishing a kinematic limitation. Hosseini et al. [11] used SPH method to simulate a dam-break flow over a dry bed. Tayebi et al. [12] proposed a predictive-corrective algorithm to solve time-dependent Navier-Stokes equations using SPH method. Leroy et al. [13] corrected the solid boundary condition in the ISPH method using a semi-analytic method. In order to find an optimal method for incompressible SPH method, Nomeritae et al. [14] discussed the various methods in this field. Their results indicated that the conventional implicit compressible methods are inefficient compared to weak compressible methods (WCSPH) due to their high computational and low-speed computing power. They proposed explicit methods to optimize the numerical approach. Ordouabadi et al. [15] used Eulerian ISPH approach to evaluate the possibility of using non-uniform particle distribution in the sensitive regions. They considered some internal flows include shear-driven cavity and flow around a circular cylinder. They concluded that the results for velocity distribution obtained from their proposed method have the same accuracy compared to ISPH and WCSPH, however, the results correspond to the pressure field have more accuracy in comparison with those schemes. Yeylaghi et al. [16] implemented an ISPH approach to simulate the fluid structure interaction (FSI). They reported that this method prevents the pressure oscillations, leading to the results that are in good agreement with the experimental data. Khayyer et al. [17] also simulated FSI using Lagrangian using ISPH and Newtonian/Hamiltonian structure models. They considered some problem for validation, including hydrostatic water column on an elastic plate. ISPH model was employed by Chow et al. [18] to simulate incompressible flows including incompressible flow around a moving square object in a cavity. They performed their simulations for $Re = 100$ and $Re = 10^6$ and reported that the runtime is a direct function of number of particles. They used serial and parallel codes to test the speed up and runtime. Bayareh et al. [19] used Lagrangian WCSPH method to simulate a dam break, submerged hatch, sandy beaches and sedimentation problems. They found that the results achieved from SPH method are in good agreement with experimental and numerical data.

It also should be considered that there are several methods for simulation of multiphase methods such as volume of Fluid (VOF) [20] and front tracking techniques [21–24].

The present work aims to simulate channel flow, channel flow with a square solid box and lid-driven cavity flow using ISPH technique. The main objective of the present paper is to evaluate the potential for the simulation of these flows from different aspects. Does the ISPH method predict the hydrodynamics of shear-thinning and shear-thickening fluids as well as Newtonian ones in channel flow? What is the accuracy of ISPH method if the Reynolds number increases in the lid-driven cavity flow?

The present paper is organized as follows: Sect. 2 describes the fundamental principles of SPH method. The governing equations are presented in Sect. 3. Section 4 presents the explicit ISPH scheme. Boundary conditions and calculation of time step are demonstrated in Sects. 5 and 6. In Sect. 7, the results are discussed and finally, concluding remarks are presented in Sect. 8.

2 SPH method

The SPH method is an interpolation approach based on the integral concept that defines each function at the interpolation points. The material is approximated by these points, named particles, which carry the properties and variables of the flow field. In SPH relations, the value of the variable A at $\vec{r}(x, y)$ is defined as the convolutional multiplication of variable A with the Dirac delta function δ [25]:

$$A(r) = \int A(r)\delta\left(\left|(r - r')\right|dr' \tag{1}$$

where the Dirac delta function δ is approximated by the kernel function $W_h\left(\left|(r - r')\right|\right)$:

$$A(r) = \int_{\Omega} A(r)W_h\left(\left|(r - r')\right|dr' \tag{2}$$

where Ω is the support area where the integration operation is performed on it. In the discrete form, Eq. 2 can be written as follows:

$$A(r_i) \approx \sum_j V_j A(r_i) W_h(r_{ij}) \tag{3}$$

where V_j denotes the volume of the particle, the index j refers to the neighboring particles i, and r_{ij} is the distance between the particles i and j. The Eq. 3 is rewritten as follows [25]:

$$A(r_i) = \sum_j m_j \frac{A(r_i)}{\rho_j} W_h(r_i - r_j, h) \tag{4}$$

The summation operation is performed on neighboring particles.

The cubic spline kernel was presented in 1992 by Monaghan [26]. The kernel is used for many problems include dam-break flows, moving a water drop with different initial velocities, deformation of waves on a gentle slope, breaking the dam and motion of water on an inclined surface. The cubic spline kernel is defined as follows:

$$W(r,h) = \alpha_D \times \begin{cases} 1 - \frac{3}{2}s^2 + \frac{3}{4}s^3 & 0 \le s < 1 \\ \frac{1}{4}(2-s)^2 & 1 \le s < 2 \\ 0 & 2 \le s \end{cases} \tag{5}$$

where $s = r/h$, r is the distance between particles, h is smoothing length, $\alpha_D = {}^{2}/_{3h}$, ${}^{10}/_{7\pi h^2}$, and ${}^{1}/_{\pi h^3}$ for one-, two-, and three-dimensional problems, respectively.

The pressure gradient is obtained using Eq. 4 as follows:

$$\vec{\nabla} P = \sum_j m_j \frac{P_j}{\rho_j} \vec{\nabla}_i W(\vec{r}_i - \vec{r}_j, h) \tag{6}$$

If the pressure gradient is written according to Eq. 6, the precision of the linear and angular momentum is not obtained. This is due to that the force acting on the particle i by a particle j does not equal the force applied to the particle j by the particle i. These forces can be symmetric by writing $\frac{\vec{\nabla} P}{\rho}$ as follows [26]:

$$\frac{\vec{\nabla} P}{\rho} = \vec{\nabla}\left(\frac{P}{\rho}\right) + \frac{P}{\rho^2}\vec{\nabla}\rho \tag{7}$$

The right hand side of Eq. 7 can be written as follows for the particle i:

$$\left(\frac{\vec{\nabla} P}{\rho}\right)_i = \sum_j m_j \frac{P_j}{\rho_j^2} \cdot \vec{\nabla}_i W_{ij} + \frac{P_i}{\rho_i^2} \sum_j m_j \cdot \vec{\nabla}_i W_{ij} \tag{8}$$

Equation 8 is simplified as follows:

$$\left(\frac{\vec{\nabla} P}{\rho}\right)_i = \sum_j m_j \left(\frac{P_j}{\rho_j^2} + \frac{P_i}{\rho_i^2}\right) \cdot \vec{\nabla}_i W_{ij} \tag{9}$$

The conservation of linear and angular momentum is satisfied if the pressure gradient is written in the form of Eq. 9. In the same way, it can be concluded that:

$$\left(\frac{1}{\rho}\nabla \cdot \vec{\tau}\right)_i = \sum_j m_j \left(\frac{\vec{\tau}_j}{\rho_j^2} + \frac{\vec{\tau}_i}{\rho_i^2}\right) \cdot \nabla_i W_{ij} \tag{10}$$

The Laplacian operator can be described as the internal multiplication of two divergence and gradient operators. In the SPH method, the solution of Navier-Stokes equations leading to pressure instability and divergence; hence, a method is used for eliminating the instability [27]:

$$\nabla \cdot \left(\frac{1}{\rho}\nabla \cdot A(r_i)\right) = \sum_j m_j \frac{8}{\rho_i^2 + \rho_j^2} \frac{A_{ij} \cdot \vec{r}_{ij} \cdot \vec{\nabla}_i W_{ij}}{\left|\vec{r}_{ij}\right|^2 + \eta^2} \tag{11}$$

where $A_{ij} = A_i - A_j$ and $\vec{r}_{ij} = \vec{r}_i - \vec{r}_j \cdot \eta$ is a small number that prevents denominator from being zero and is usually equal to 0.1 h.

3 Governing equations

The governing equations for fluid flow in the Lagrangian framework are as follows [11]:

$$\frac{1}{\rho}\frac{D\rho}{Dt} + \nabla \cdot \vec{u} = 0 \tag{12}$$

$$\frac{D\vec{u}}{Dt} = \vec{g} - \frac{1}{\rho}\vec{\nabla} P + \frac{1}{\rho}\nabla \cdot \vec{\tau} \tag{13}$$

where $\vec{u}$ is the velocity field, t is the time, ρ is the density, P is the pressure, $\vec{\tau}$ is the stress tensor and $\vec{g}$ is the acceleration of gravity. Also, D/Dt is material derivative.

The Momentum equation has three terms including the pressure gradient, velocity divergence and gravitational force. The above equations must be solved at any time for all particles.

To solve non-Newtonian fluid flow, it is needed to define the stress tensor [28]:

$$\tau = \mu_{eff}(|D|)D \tag{14}$$

where D is the deformation rate tensor and $|D|$ represents the second invarient of the strain tensor D (deformation) and is expressed as follows:

$$D = \nabla u + \nabla u^T \tag{15a}$$

$$D = \begin{bmatrix} 2\frac{\partial u}{\partial x} & \frac{\partial u}{\partial y} + \frac{\partial v}{\partial x} \\ \frac{\partial u}{\partial y} + \frac{\partial v}{\partial x} & 2\frac{\partial v}{\partial y} \end{bmatrix} \tag{15b}$$

$$|D| = \sqrt{\frac{1}{2}\sum_{ij} D_{ij}D_{ij}} \tag{15c}$$

or

$$|D| = \sqrt{2\left(\frac{\partial u}{\partial x}\right)^2 + 2\left(\frac{\partial v}{\partial y}\right)^2 + \left(\frac{\partial u}{\partial y} + \frac{\partial v}{\partial x}\right)^2} \tag{16}$$

$\partial u/\partial x$ and $\partial u/\partial y$ should be expressed as SPH approach:

$$\left(\frac{\partial u}{\partial x}\right)_i = \sum_i \frac{m_i}{\rho_i}(u_j - u_i)\frac{x_i - u_j}{\left|r_{ij}\right|}\frac{dW}{dr_{ij}} \tag{17a}$$

$$\left(\frac{\partial u}{\partial y}\right)_i = \sum_i \frac{m_i}{\rho_i}(u_j - u_i)\frac{y_i - y_j}{\left|r_{ij}\right|}\frac{dW}{dr_{ij}} \tag{17b}$$

Similarly, $\partial v/\partial x$ and $\partial v/\partial y$ are also obtained.

Now, the non-Newtonian power low model used in the present study is described. The effective viscosity of this model is defined as [28]:

$$\mu_{eff}(|D|) = \mu|D|^{n-1} \tag{18}$$

where μ and n are the fluid viscosity and the power law index, respectively. $n < 1$ shows the pseudoplastic (shear-thinning) fluids, $n = 1$ indicates the Newtonian fluid, and $n > 1$ refers to the dilatant (shear-thickening) fluids.

4 Explicit three-step SPH algorithm

In the first step of the explicit three-step incompressible method, the momentum equation is solved by taking into account the gravitational acceleration without considering any other force. Hence [11]:

$$\begin{cases} u^* = u_{t-\Delta t} + g_x\Delta t \\ v^* = v_{t-\Delta t} + g_y\Delta t \end{cases} \tag{19}$$

where u^* and v^* are the middle velocities obtained from the first step. In the second step, these velocities are used to calculate the divergence of the stress tensor. According to Eq. 10, it can be written:

$$\left(\frac{1}{\rho}\nabla\cdot\tau\right) = \sum_j m_j\left(\frac{\tau_i}{\rho_i^2} + \frac{\tau_j}{\rho_j^2}\right)\nabla_i W(r_{ij}, h) = S = s_x i + s_y j \tag{20}$$

At the end of the second step, the velocities and particle positions are updated as follows:

$$\begin{cases} u^{**} = u^* + s_x\Delta t = u_{t-\Delta t} + g_x\Delta t + s_x\Delta t \\ v^{**} = v^* + s_y\Delta t = v_{t-\Delta t} + g_y\Delta t + s_y\Delta t \end{cases} \tag{21}$$

$$\begin{cases} x^* = u_{t-\Delta t} + u^{**}\Delta t \\ y^* = v_{t-\Delta t} + v^{**}\Delta t \end{cases} \tag{22}$$

Until this step, no condition has been imposed for fluid incompressibility. Therefore, in the third step, the middle density of particles can be calculated using the continuity equation [11]:

$$\rho^* = \rho_0 + \left(\sum_j m_j(u_i - u_j)\cdot\nabla_i W(r_{ij}, h)\right) \tag{23}$$

where ρ^* is the instantaneous fluid density up to the end of the initial prediction stage and ρ_0 is the constant density of the fluid. Now, the velocity field must be calculated again for particles to return the particles density to its original state. For this purpose, the pressure gradients in the momentum equation are combined with the continuity equation:

$$\begin{cases} \frac{1}{\rho_0}\frac{\rho_0 - \rho^*}{\Delta t} + \nabla\cdot(\hat{V}) = 0 \\ \hat{V} = -\left(\frac{1}{\rho^*}\nabla P\right)\Delta t \end{cases} \tag{24}$$

where $\hat{V}$ is the corrective velocity. By combining these equations, the Poisson equation is obtained as follows:

$$\nabla\cdot\left(\frac{1}{\rho^*}\nabla P_{t+\Delta t}\right) = \frac{\rho_0 - \rho^*}{\Delta t^2} \tag{25}$$

The Eq. 25 is written as SPH approach:

$$P_i = \left(\frac{\rho_0 - \rho^*}{\Delta t^2} + \sum_j \frac{8m_j}{(\rho_i + \rho_j)^2}\frac{P_j\vec{r}_{ij}\cdot\nabla_i W_{ij}}{\left|r_{ij}\right|^2 + \eta^2}\right) \times \left(\sum_j \frac{8m_j}{(\rho_i + \rho_j)^2}\frac{\vec{r}_{ij}\cdot\nabla_i W_{ij}}{\left|r_{ij}\right|^2 + \eta^2}\right)^{-1} \tag{26}$$

The corrective velocity is obtained using Eq. 26 and the pressure of each particle:

$$\hat{V}_i = -\Delta t\sum_j m_j\left(\frac{P_j}{\rho_j^2} + \frac{P_i}{\rho_i^2}\right)\nabla_i W_{ij} \tag{27}$$

At the end of step 3, the final velocity of the particles is calculated as follows:

$$u_{t-\Delta t} = u^{**} + \hat{u}$$
$$v_{t-\Delta t} = v^{**} + \hat{v} \quad (28)$$

The final position of particles is also obtained by using a central difference approach [11]:

$$x_t = x_{t-\Delta t} + \frac{\Delta t}{2}\left(u_t + u_{t-\Delta t}\right)$$
$$y_t = y_{t-\Delta t} + \frac{\Delta t}{2}\left(v_t + v_{t-\Delta t}\right) \quad (29)$$

This process is performed for all particles.

5 Boundary conditions

Solid boundary particles are the same as the fluid particles, however the velocity of these particles is set zero at the end of each time. Hence, the position of these particles remains constant during the simulations. The Poisson equation of the pressure is solved for boundary particles. Therefore, the pressure of each particle does not change with the approaching or moving away of other particles. For example, as the fluid particles move towards the solid boundary particles, the pressure of solid particles increases. Boundary particles exert a repulsive force on the liquid particles. This force prevents the liquid and boundary particles from collapsing. Since the particle velocity of the solid boundary is zero at the end of each step, the no-slip boundary condition is applied correctly.

6 Calculation of the time step

Like other computational fluids dynamics, the SPH method requires a reasonable particle size to achieve the accuracy of the results. Because the internal fluid particles are discrete particles, they cannot be deformed like a real fluid. Therefore, the number of these particles should be sufficiently chosen to simulate the actual fluid flow and also to obtain the necessary numerical convergence. Sustainability analysis is used to find the appropriate step time values. The time interval Δt should satisfy the Courant condition [29]:

$$\Delta t \leq 0.1 \frac{l_0}{V_{max}} \quad (30)$$

where V_{max} is the maximum particle velocity in each time step. The coefficient 0.1 ensures that the particles move only a small distance in comparison with h in each time step. Another limitation for the time step comes from the explicit finite-difference method for simulating the diffusion problem, which applies the following relation:

$$\Delta t \leq \beta \frac{l_0^2}{\mu_{eff}/\rho} \quad (31)$$

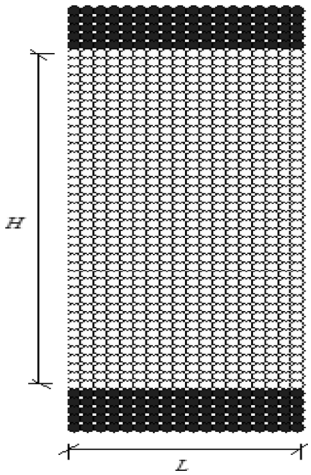

Fig. 1 A schematic of the channel flow

β is a coefficient that depends on kernel and the initial arrangement of particles. It is usually obtained by numerical simulations and is of the order of 0.1. The effective viscosity μ_{eff} is calculated using a simple Newtonian model. An acceptable time step should satisfy both of the above conditions.

7 Results

In this section, first, the two-dimensional flow in a channel for the Newtonian and non- Newtonian power law fluids is considered and the results are compared to the analytical solution. Then, the channel flow in the presence of a square solid object is simulated and the velocity profile. Finally, the flow in a cavity with a moving cap is studied and verified by the numerical simulations. All simulations presented in the present work are performed by a FORTRAN code.

7.1 Two-dimensional fluid flow in a channel

Now, the explicit three-step ISPH method is employed to simulate the flow in a two-dimensional channel. The width of the channel is H and the fluid is water (the density $\rho = 1000$ kg/m^3 and dynamic viscosity $\mu = 0.01$ pa s). The gravity acceleration is assumed to be negligible. Figure 1 shows the initial distribution of particles and geometry of the channel. The black circles indicate the solid boundary (five layers for each boundary) and the white circles illustrate the fluid particles.

To solve this problem, 592 fluid particles with five layers of boundary particle are used. The initial distance of the particles is $L = 0.03$ m, the smoothing length is $h = 1.5$ L_0 and dimensionless length of the channel is $L/H = 1/2$.

A periodic boundary condition is used in the horizontal direction of the flow. The no-slip boundary condition is imposed on the upper and lower walls. The propulsion force required to create the flow is provided by applying the volumetric force (gravitational acceleration in the horizontal direction) for the entire particle in the momentum equation. The Reynolds number is defined based on the maximum input velocity (u_{max}) and channel width (H) and kinematic viscosity (v):

$$Re = \frac{u_{max}H}{v} = 5 \tag{32}$$

An analytical solution of the fully developed horizontal velocity profile for the channel flow is [30]:

$$u(y) = 4u_{max}y(H - y)/H \tag{33}$$

According to Eq. 33, the analytic solution does not depend on the Reynolds number. The numerical results obtained using ISPH method for the water fluid with $U = u/u_{max}$ are presented in Fig. 2 in comparison with the analytical solution. The present results are in very good agreement with the analytical ones.

As shown in Fig. 2, the fluid has the maximum velocity at the center of the channel and its velocity on solid walls is zero. The shape of the parabolic profile drawn in Fig. 2 corresponds to the region in which the flow has reached a fully developed state.

Now, the simple channel flow is investigated for non-Newtonian power law fluids. The constitutive equation was described in Sect. 3. The geometry and initial distribution of the particles are shown in Fig. 1, with the difference that dimensionless length of the channel $L/H = 1$ is considered. The rest of the conditions are the same as the previous one. For a non-Newtonian power law fluid flow in a channel, there is an analytical solution for fully developed horizontal velocity profile [31]:

$$u(y) = \left(\frac{2n+1}{n+1}\right)\left(1 - (2y)^{1+1/n}\right) \tag{34}$$

According to Eq. 34, the analytic solution does not depend on the Reynolds number. The $U = u/u_{max}$ obtained using ISPH method for a shear-thinning fluid ($n = 0.5$) and a shear-thickening fluid ($n = 1.5$) and also a Newtonian one ($n = 1.0$) is compared with the analytical solution and presented in Fig. 3. The present results are in very good agreement with the analytical ones.

The number of particles used for this case is 2640 particles. It is observed that for a shear-thinning fluid ($n = 0.5$), the velocity increases near the wall, and therefore the velocity gradient yields a higher value than the shear-thickening fluid ($n = 1.5$). As a result, for a mean value of the speed given in the channel, the velocity decreases near the line of symmetry (Fig. 4). The results reveal that the maximum velocity decreases with the power law index. As the power low increases, the effective viscosity increases, leading to more resistance against the fluid flow. These results for different fluids are compared in Fig. 4. More iteration is needed to achieve convergence by decreasing the power law index n and sometimes the convergence will not be achieved.

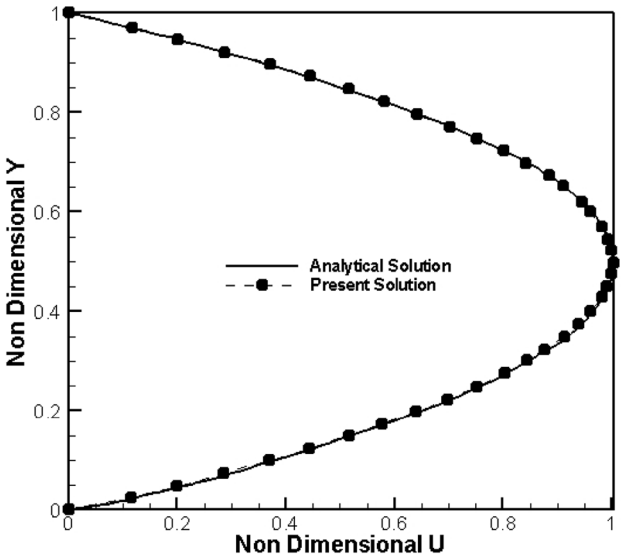

Fig. 2 Comparison of non-dimensional velocity profile u/u_{max} for simple channel flow computed by the ISPH with analytical solution

The effect of the number of initial particles on the horizontal velocity profile in comparison with the analytical solution results for Newtonian fluids in Fig. 5 indicates the accuracy of this method. The figure demonstrates that the solution with a particle number of 2640 is better than that with 1320 particles. It should be pointed out that as the particle number increases, more accurate results will be achieved.

7.2 The flow in a two-dimensional channel in the presence of a solid object

In the previous section, the flow in a two-dimensional channel was investigated. In this section, the flow in a two-dimensional channel with a rectangular solid body having a length of 925.0 and a width of 975.0 m is investigated. The geometry of the problem is shown in Fig. 6. No-slip boundary condition is imposed on the solid boundary. The symmetry boundary condition is used at $y = \pm L$. In the SPH method, the application of this boundary condition is simpler than other conditions. On the other hand, in the geometries where the flow pattern is repeated, this boundary condition reduces the computational time.

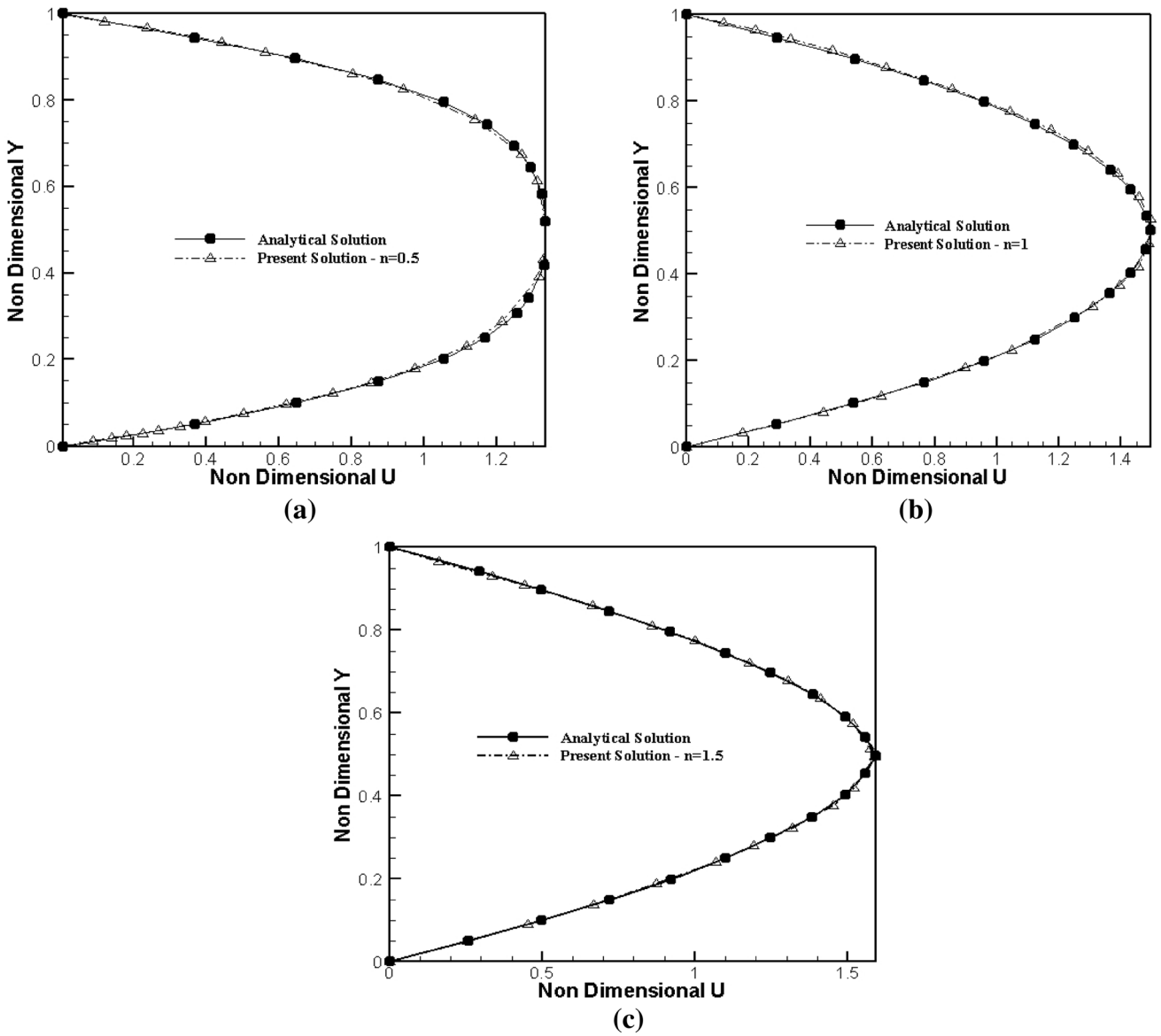

Fig. 3 Comparison of non-dimensional velocity profile u/u_{max} for simple channel flow computed by the ISPH with analytical solution: **a** $n = 0.5$, **b** $n = 1$, and **c** $n = 1.5$

Other flow characteristics are the same as mentioned in 7.1. In Fig. 7, $U = u/u_{max}$ profile is plotted for water fluid. There is a discontinuity in the velocity profile due to the presence of solid obstacle. As shown in Fig. 9, the velocity is zero in the range of 0.25–0.47.

7.3 The lid-driven square cavity flow

The flow inside a lid-driven square cavity is a known problem of incompressible flow that is used to validate numerical methods. The two-dimensional square cavity with the length of L contains a stationary fluid. Its lid has a constant velocity U. The gravitational force is neglected.

Due to the motion of the upper wall, the fluid flows into the container and a certain shape of the fluid is expected depends on the Reynolds number. The initial arrangement of the particles and its geometry are shown in Fig. 8. The wall includes five layers of boundary particles, so the liquid particles do not penetrate the wall. For three stationary walls, since the velocity and displacement at each step are zero, no-slip boundary condition is applied correctly. 1600 fluid particles are used in this simulation. The initial distance between the particles is $L_0 = 0.03$ m. The Reynolds number is defined as $Re = \frac{\rho U_{lid} L}{\mu}$ in which ρ is the fluid density, U_{lid} is the upper wall

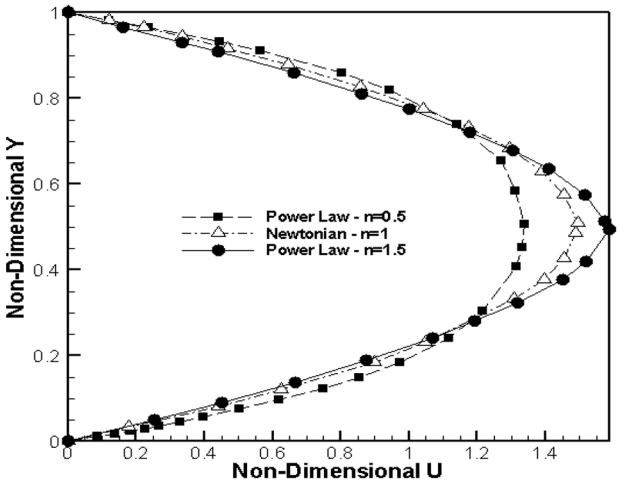

Fig. 4 Comparison of non-dimensional velocity profile u/u_{max} for non-Newtonian power law fluids with $n = 0.5$, 1.0 and 1.5

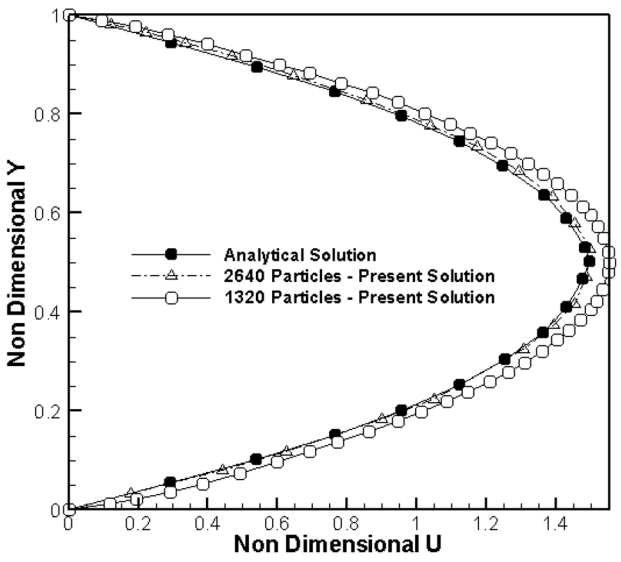

Fig. 5 Effect of the number of particles on the velocity profile u/u_{max} for a non-Newtonian power law fluid ($n = 1.5$)

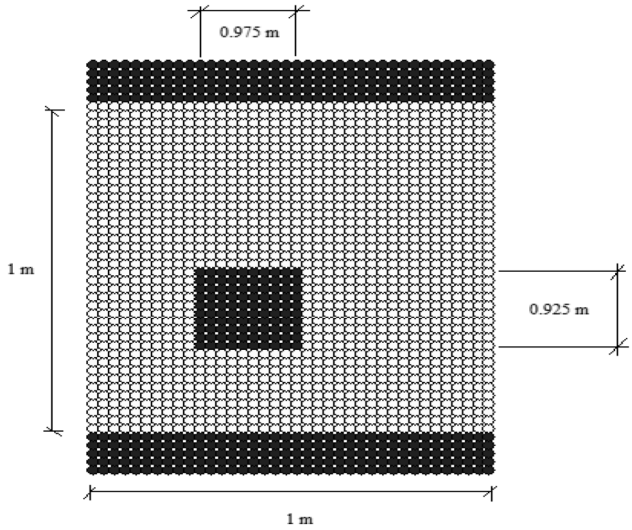

Fig. 6 A schematic of the channel flow in the presence of a rectangular object

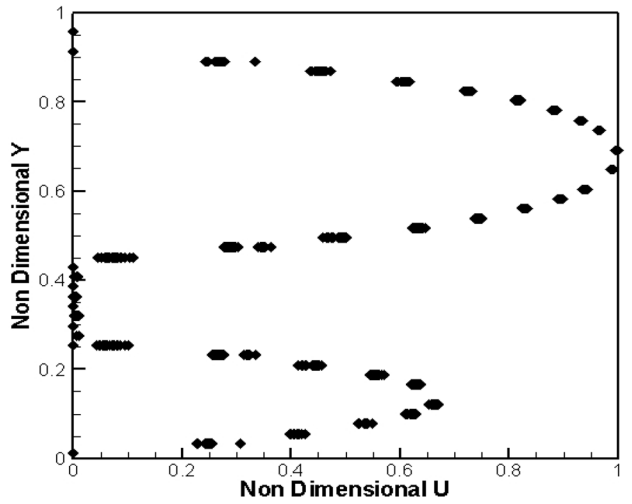

Fig. 7 The velocity profile u/u_{max} for water flow in a channel in the presence of an obstacle

velocity, L is the square side and μ is the dynamic viscosity of the fluid. In Fig. 8, the black circles represent the solid boundary and gray circles indicate fluid particles. For solid particles, shear stresses, velocity and displacement are zero, except for upper wall particles that have constant velocity U. The cavity problem for the Newtonian fluid (water) is solved for three Reynolds numbers Re = 100, 400 and 1000. The results are verified by the results of Ghia et al. [32] who used multi-grid approach to perform their simulations. The velocity is non-dimensionalized by U_{lid}.

In Fig. 9, the non-dimensional horizontal velocity is plotted for water at Re = 100 as a function of y-direction at x = 0.5. As shown in the figure, the results of the SPH method are in very good agreement with Ghia et al. [32]. After about 6000 time steps, the flow reach steady state. Due to the proper performance of the boundary condition, the particles do not exit from the walls during the simulation. While in similar methods, there is the possibility of exiting particles from the computational domain in the upper corners of the cavity usually. At these points, the discontinuity at the velocity creates a singularity of pressure.

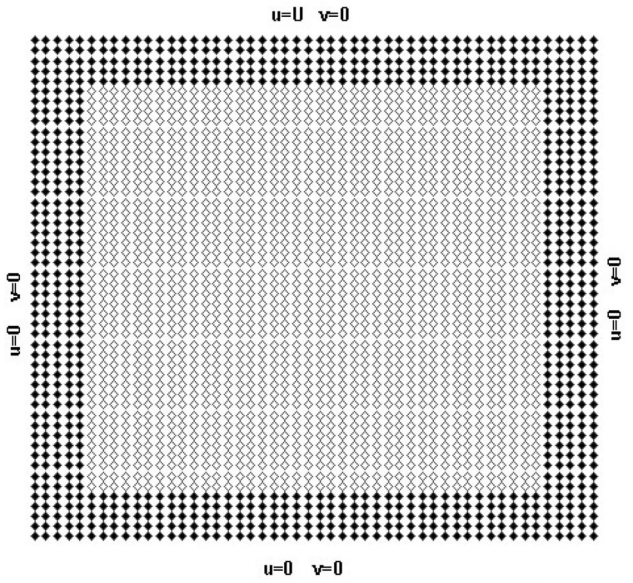

Fig. 8 Initial arrangement of particles for Lid-driven cavity flow

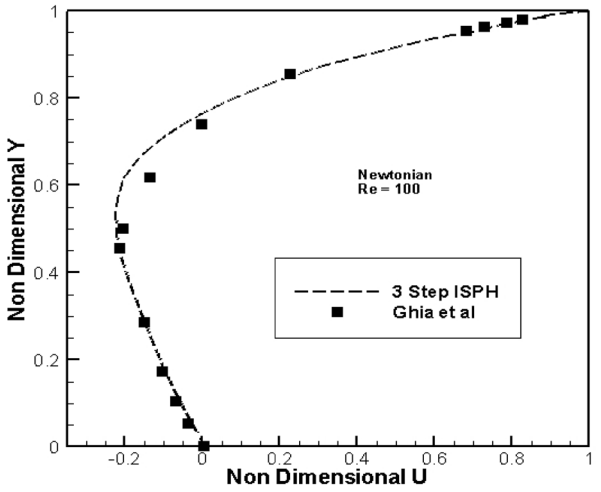

Fig. 9 Dimensionless horizontal *U* velocity for Lid-driven flow at Re = 100 and x = 0.5 using 40 × 40 particles

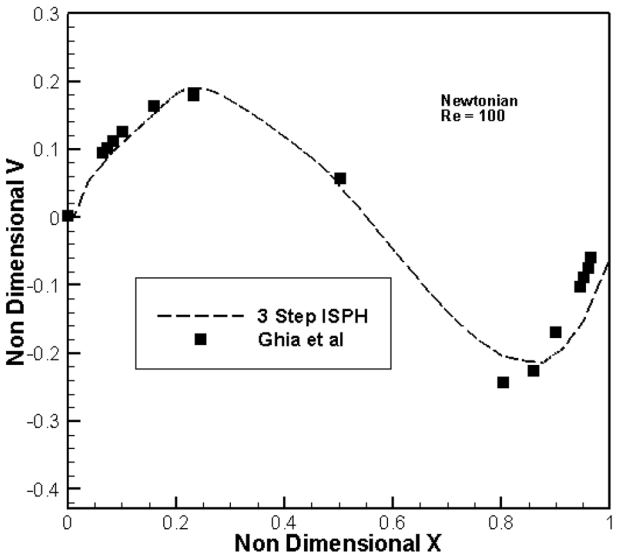

Fig. 10 Dimensionless vertical *V* velocity for Lid-driven flow at Re = 100 and x = 0.5 using 40 × 40 particles

Figure 10 compares the vertical velocity at x = 0.5 line for the water fluid for the Reynolds number Re = 400. The results are in good agreement with the ones of Ghia et al. [32]. The difference between the results of the present method and their results is due to the large number of particles that they used for their simulations (they used multi-grid method with 129 × 129 grid resolution).

In Fig. 11, the stream function of the present solution is presented in comparison with the results of Ghai et al. [32] for the water fluid at Re = 100. Two small vortices are created at the bottom of the cavity and a vortex at a position of x = 0.6 and y = 0.7.

The results for Re = 400 are now being investigated. In Fig. 12, the dimensionless horizontal velocity is plotted versus y-position at x = 0.5. The present results are in a good agreement between the results of the SPH method and the results of Ghia et al. [32]. Also, Fig. 13 compares the vertical velocity at x = 0.5.

In Fig. 14, the stream function obtained from the SPH method for Re = 400 are compared with those presented by Ghia et al. [32]. It is observed that the middle vortex is created in the center of the square and the lower right-hand vortex is larger than that of Re = 100.

The simulations are repeated for the Reynolds number of 1000. Figures 15, 16, 17 show dimensionless horizontal velocity, dimensionless vertical velocity, and stream function, respectively. These results demonstrate that the results of the ISPH method are in good agreement with results of Ghia et al. [32] for the Reynolds numbers of 100 and 400. However, it is demosntrated that the simulation with1600 particles cannot predict the behavior of lid-driven cavity flow for Re = 1000 properly. The simulation is performed using 80 × 80 particles and it is revealed that this grid resolution is sufficient for prediction of flow hydrodynamics. It should be noted that the middle vortex is generated approximately in the center of the cavity and the vortex of the left side of the bottom is larger than the previous cases (Re = 100 and 400).

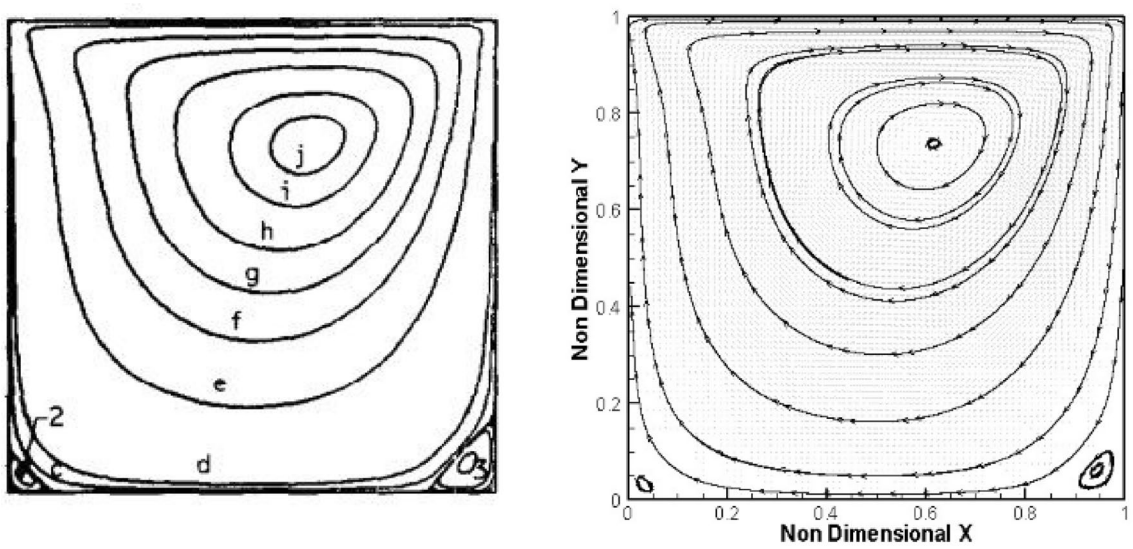

Fig. 11 Streamlines for lid-driven cavity flow at $Re = 100$: Ghia et al. [32] (left) and the ISPH method using 40×40 particles (right)

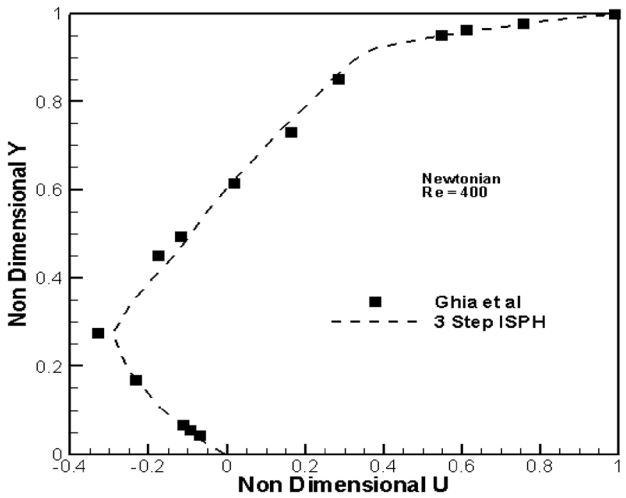

Fig. 12 Dimensionless horizontal U velocity for Lid-driven flow at Re = 400 and x = 0.5 using 40×40 particles

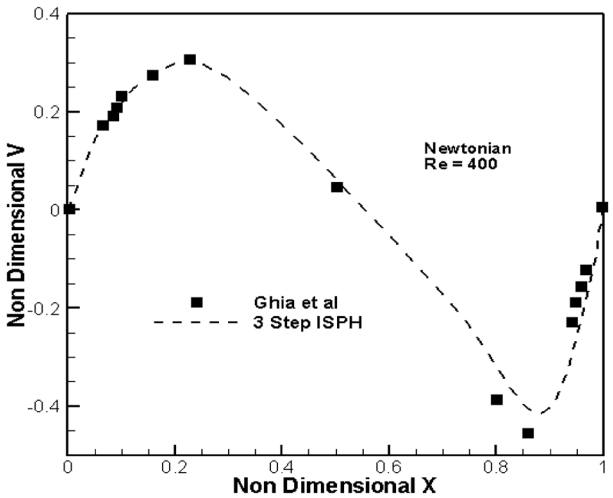

Fig. 13 Dimensionless vertical V velocity for Lid-driven flow at Re = 400 and x = 0.5 using 40×40 particles

8 Conclusions

In this paper, three fluid mechanics problems were verified by using an explicit three-step ISPH method. The channel flow problem for the Newtonian fluid (water) was studied and the velocity profile for fully developed region was analyzed by analytical solution. In addition, non-Newtonian power law fluid flow in a channel was investigated for different power law indices and the results were compared with the analytical solution. In the second part, the flow in a channel in the presence of a solid obstacle was investigated. The velocity profile showed a discontinuity in the velocity field around the solid object. In the last part, the lid-driven cavity

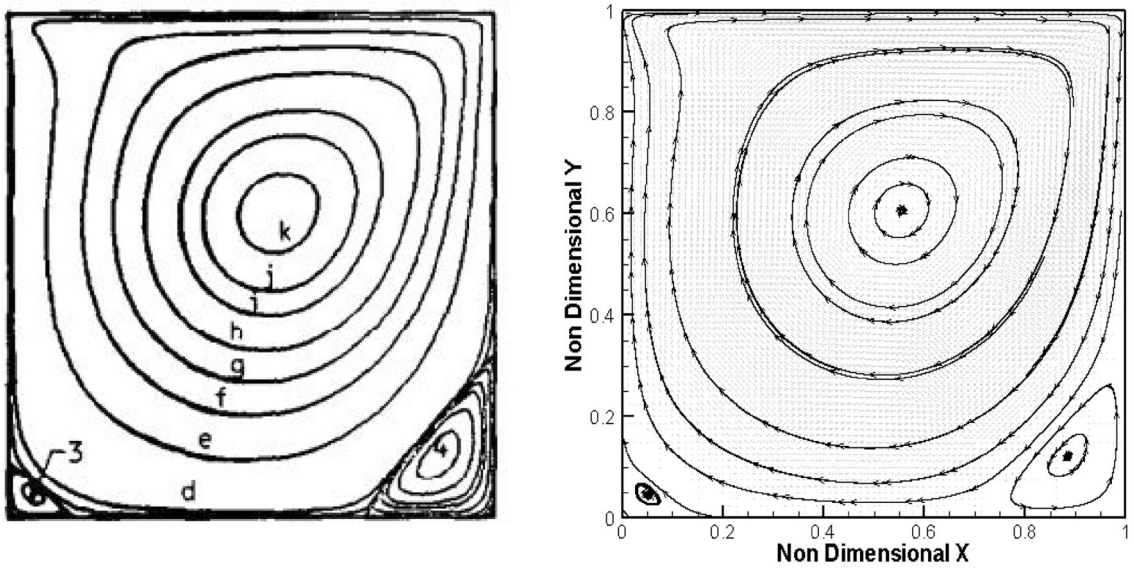

Fig. 14 Streamlines for lid-driven cavity flow at *Re* = 400: Ghia et al. [32] (left) and the ISPH method using 40 × 40 particles (right)

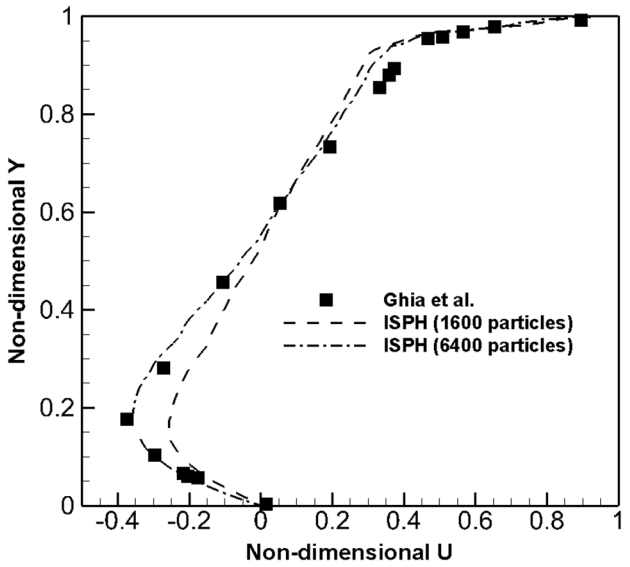

Fig. 15 Dimensionless horizontal *U* velocity for lid-driven flow at Re = 1000 and x = 0.5 using 40 × 40 and 80 × 80 particles

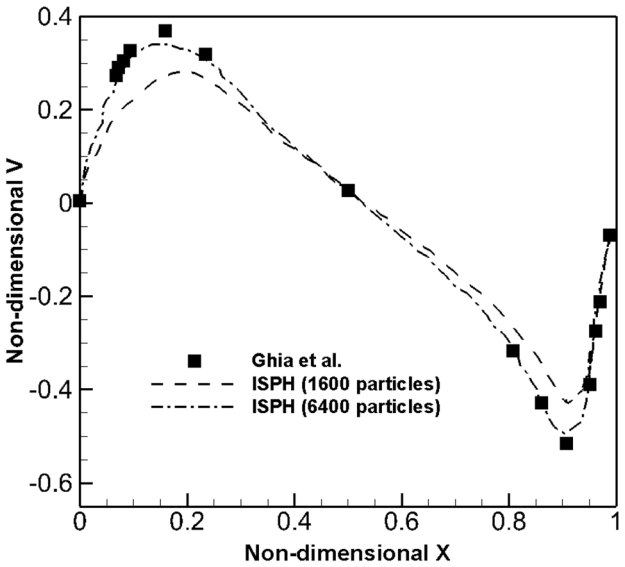

Fig. 16 Dimensionless vertical *V* velocity for lid-driven flow at Re = 1000 and x = 0.5 using 40 × 40 and 80 × 80 particles

flow was studied for a Newtonian fluid (water) at *Re* = 100, 400, and 1000. The horizontal and vertical velocity profiles in the middle plane and also the stream function were compared to the results of Ghia et al. [32]. The results reveal that only 1600 particles are required for reasonable prediction of lid-driven square cavity flow at Re = 100 and 400 and 6400 particles is required to predict it at Re = 1000. It can be concluded that the ISPH method has a high ability to model non-Newtonian fluid flows and is more accurate than the WCSPH method due to much less pressure fluctuations during the simulations [18, 19].

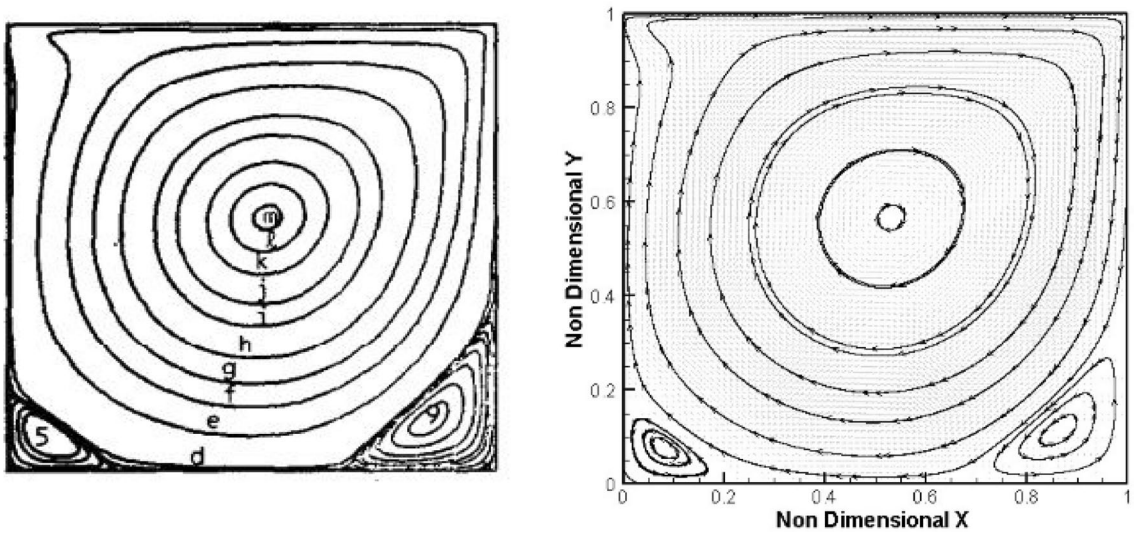

Fig. 17 Streamlines for lid-driven cavity flow at $Re = 1000$: Ghia et al. [32] (left) and the ISPH method using 40×40 particles (right)

Compliance with ethical standards

Conflict of interest The authors declare that they have no competing interests.

References

1. Lucy LB (1977) A numerical approach to the testing of the fission hypothesis. Astron J 82:1013–1024
2. Gingold RA, Monaghan JJ (1977) Smoothed particle hydrodynamics: theory and application to non-spherical stars. Mon Not R Astron Soc 181(3):375–389
3. Monaghan JJ (1985) Particle methods for hydrodynamics. Comput Phys Rep 3(2):71–124
4. Monaghan JJ (1994) Simulating free surface flows with SPH. J Comput Phys 110(2):399–406
5. Takeda H, Miyama SM, Sekiya M (1994) Numerical simulation of viscous flow by smoothed particle hydrodynamics. Prog Theor Phys 92(5):939–960
6. Morris JP, Fox PJ, Zhu Y (1997) Modeling low Reynolds number incompressible flows using SPH. J Comput Phys 136(1):214–226
7. Monaghan JJ (2000) SPH without a tensile instability. J Comput Phys 159(2):290–311
8. Monaghan JJ (2002) SPH compressible turbulence. Mon Not R Astron Soc 335(3):843–852
9. Liu M, Meakin P, Huang H (2007) Dissipative particle dynamics simulationof pore-scale multiphase fluid flow. Water Resour Res 43:W04411
10. Ellero M, Serrano M, Espanol P (2007) Incompressible smoothed particle hydrodynamics. J Comput Phys 226(2):1731–1752
11. Hosseini S, Manzari M, Hannani S (2007) A fully explicit three-step SPH algorithm for simulation of non-Newtonian fluid flow. Int J Numer Meth Heat Fluid Flow 17(7):715–735
12. Tayebi A, Dehkordi BG (2013) Development of a PISO-SPH method for computing incompressible flows. Proc Inst Mech Eng Part C J Mech Eng Sci 228(3):481–490
13. Leroy A, Violeau D, Ferrand M, Kassiotis C (2014) Unified semi-analytical wall boundary conditions applied to 2-D incompressible SPH. J Comput Phys 261:106–129
14. Nomeritae N, Daly E, Grimaldi S, Bui HH (2016) Explicit incompressible SPH algorithm for free-surface flow modelling: a comparison with weakly compressible schemes. Adv Water Resour 97:156–167
15. Ordoubadi M, Farhadi A, Yeganehdoust F, Emdad H, Yaghoubi M, Rad E, Goshtasebi A (2016) Eulerian ISPH Method for Simulating Internal Flows. J Appl Fluid Mech 9(3):1477–1490
16. Yeylaghi S, Moa B, Oshkai P, Buckham B, Crawford C (2016) ISPH modelling of an oscillating wave surge converter using an OpenMP-based parallel approach. J Ocean Eng Mar Energy 2(3):301–312
17. Khayyer A, Gotoh H, Falahaty H, Shimizu Y (2018) Towards development of enhanced fully-Lagrangian mesh-free computational methods for fluid-structure interaction. J Hydrodyn 30(1):49–61
18. Chow AD, Rogers BD, Lind SJ, Stansby PK (2018) Incompressible SPH (ISPH) with fast Poisson solver on a GPU. Comput Phys Commun 226:81–103
19. Bayareh M, Nourbakhsh A, Rouzbahani F, Tafreshi MK (2019) Simulation of sand particles flow using a weakly compressible smoothed particle hydrodynamics method (WCSPH). Annales de Chimie: Science des Materiaux 43:43–45
20. Goodarzi Z, Ahmadi Nadooshan A, Bayareh M (2018) Numerical investigation of off-centre binary collision of droplets in a horizontal channel. J Braz Soc Mech Sci Eng 40:1–10
21. Bayareh M, Mortazavi S (2011) Effect of density ratio on the hydrodynamic interaction between two drops in simple shear flow. Iran J Sci Technol 35:441–452
22. Bayareh M, Mortazavi S (2013) Equilibrium position of a buoyant drop in Couette and Poiseuille flows at finite Reynolds numbers. J Mech 29:53–58
23. Bayareh M, Mortazavi S (2009) Geometry effects on the interaction of two equal-sized drops in simple shear flow at finite Reynolds numbers. 5th Int Conf Computat Methods Multiphase Flow WIT Trans Eng Sci 63:379–388. https://doi.org/10.2495/MPF090321
24. Bayareh M, Mortazavi S (2010) Migration of a drop in simple shear flow at finite Reynolds numbers: size and viscosity ratio effects. In: Proceeding of international conference

on mechanical, industriel and manufacturing engineering (ICMIME), Cape Town, South Africa
25. Monaghan JJ (2005) Smoothed particle hydrodynamics. Rep Prog Phys 68(8):1703
26. Monaghan JJ, Cas R, Kos A, Hallworth M (1999) Gravity currents descending a ramp in a stratified tank. J Fluid Mech 379:39–69
27. Cummins SJ, Rudman M (1999) An SPH projection method. J Comput Phys 152(2):584–607
28. Xenakis A, Lind S, Stansby P, Rogers B (2015) An incompressible SPH scheme with improved pressure predictions for free-surface generalised Newtonian flows. J Nonnewton Fluid Mech 218:1–15
29. Shao S, Lo EY (2003) Incompressible SPH method for simulating Newtonian and non-Newtonian flows with a free surface. Adv Water Resour 26(7):787–800
30. Schäfer M, Turek S, Durst F, Krause E, Rannacher R (1996) Benchmark computations of laminar flow around a cylinder. Springer, Berlin
31. Yoshino M, Hotta Y, Hirozane T, Endo M (2007) A numerical method for incompressible non-Newtonian fluid flows based on the lattice Boltzmann method. J Nonnewton Fluid Mech 147(1):69–78
32. Ghia U, Ghia KN, Shin C (1982) High-Re solutions for incompressible flow using the Navier-Stokes equations and a multigrid method. J Comput Phys 48(3):387–411